THE JOURNAL OF PHYSICAL CHEMISTRY C

Article

Cite This: J. Phys. Chem. C 2019, 123, 30746−30753

pubs.acs.org/JPCC

# Pressure-Induced Polymerization of Monosodium Acetylide: A Radical Reaction Initiated Topochemically

Jun Han,[†] Xingyu Tang,[†] Yida Wang,[†] Yajie Wang,[†] Yehua Han,[∥] Xiaohuan Lin,[†] Xiao Dong,[‡] Hyun Hwi Lee,[§] Haiyan Zheng,*[,†] Kuo Li,*[,†] and Ho-kwang Mao[†]

[†]Center for High Pressure Science and Technology Advanced Research, 10 Xibeiwang East Road, Haidian, Beijing 100094, China

[∥]State Key Laboratory of Heavy Oil Processing, College of Chemical Engineering and Environment, China University of Petroleum-Beijing, No. 18 Fuxue Road, Changping, Beijing 102249, China

[‡]Key Laboratory of Weak-Light Nonlinear Photonics, School of Physics, Nankai University, Tianjin 300071, China

[§]Pohang Accelerator Laboratory, POSTECH, Pohang 790-784, Republic of Korea

Supporting Information

**ABSTRACT:** Pressure-induced polymerization (PIP) of metal acetylides is a novel method to synthesize a metal−carbon framework and polycarbide materials with unique structures and properties. However, the pressure required for the PIP of $C_2^{2-}$ is too high for large-scale synthesis. In this work, we investigated the PIP of monosodium acetylide ($NaC_2H$) by performing in situ Raman spectroscopy, infrared spectroscopy, X-ray diffraction, and impedance spectroscopy up to 30 GPa and ex situ gas chromatography−mass spectrometry on the recovered sample. $NaC_2H$ experiences a phase transition at 7 GPa and polymerizes at 14 GPa, which is the lowest PIP pressure of acetylide to date and already in the working range of a large volume press. At the reaction threshold, the nearest intermolecular C···C distance is about 2.9 Å, which is almost the same as that of $CaC_2$ and indicates a topochemical initiation. The PIP is mainly a free radical addition process. The termination of the free radicals limits the composition of the produced polycarbide anions $C_xH_y^{n-}$ within $x - 2 \le y + n \le x + 2$. Our work discloses the threshold of the intermolecular distance for the PIP of acetylide and proposes the reaction mechanism, which furthers the investigation of its high-pressure chemical reaction.

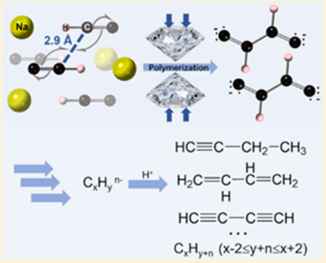


## INTRODUCTION

Conductive metal polycarbides have attracted extensive attention due to their excellent structural and electronic properties[1] and have potential applications in battery electrodes, superconductors, and other technological materials.[2,3] The carbon atoms bond to each other to form various frameworks, and the metal cations tune the charges and properties. Under high pressure, many new metal polycarbides have been predicted and synthesized, such as one-dimensional carbon chains, quasi-two-dimensional carbon nanoribbons, and structures with three-dimensional skeletons.[4−15] It was predicted that under high pressure, metal acetylides such as $MgC_2$ and $BeC_2$ could transfer into interconnected five-membered carbon ring structures,[5] while $Li_2C_2$ and $CaC_2$ would form chain, ribbon, and graphitic structures.[6−9] 3D framework structures might be obtained from metal graphenide starting materials, such as $LiC_6$ and $CaC_6$.[10−12] Such transition processes from isolated dumbbells or graphite layers are referred to as pressure-induced polymerization (PIP).

Experimentally, the PIP of $CaC_2$ and $Li_2C_2$ acetylides are well demonstrated. Linear and cyclic structures were detected in the products recovered from high pressure.[13−15] $Li_2C_2$ polymerized to form a ribbon structure under high pressure at room temperature, with its conductivity enhanced $10^9$-fold.[13] Under pressure above 27 and 36 GPa and high-temperature conditions, $Li_2C_2$ forms lithium graphenide ($LiC_2$) and lithium polyacenide ($Li_3C_4$), respectively, which are recognized as the widest and narrowest nanoribbon with a zigzag edge.[14] The PIP of acetylide enhances the conductivity significantly, which is important for Li battery materials and other applications. However, the pressure required for the PIP of carbide is very high, typically around 22 GPa for $CaC_2$ and even 35 GPa for $Li_2C_2$, due to the repulsion of the electrostatic interaction and blocking of the cations during compression.[13,15] In contrast, the polymerization pressure of the neutral acetylene molecular crystal is around 3.5 GPa,[16] much lower than that of the acetylides. This suggests that the PIP would be facilitated by reducing the charges of the anions and number of cations.

In this work, monosodium acetylide ($NaC_2H$), composed of $Na^+$ and H—C≡$C^-$ monovalent anions, was investigated up to 30 GPa. It was expected that this unsymmetrical precursor would produce exotic carbon structures different from those of $C_2^{2-}$, and the lower charge density will decrease the reaction pressure. By performing in situ Raman and IR spectroscopy up to 30 GPa, we found that $NaC_2H$ polymerized at around 14 GPa, much lower than $CaC_2$ and $Li_2C_2$. The PIP was accompanied by an enhancement of conductivity of more

Received: October 15, 2019
Revised: November 12, 2019
Published: November 13, 2019






DOI: 10.1021/acs.jpcc.9b09698
J. Phys. Chem. C 2019, 123, 30746−30753

than $10^2$-fold. The Rietveld refinement data of the X-ray diffraction (XRD) show that the intermolecular distance is about 2.9 Å, which is almost the same as that of $CaC_2$,[15] and the reaction route is proposed based on the topochemical analysis and the gas chromatography−mass spectrometry (GC−MS) result.

## METHODS

**Sample Preparation.** $NaC_2H$ suspension (18 wt % in dimethylbenzene) was purchased from Aladdin and heated in a glovebox at 100 °C to remove the solvent. No impurity was detected in the powder XRD data collected on the PANalytical Empyrean diffractometer (Cu $K_\alpha$ radiation; $\lambda$ = 1.5418 Å). Rietveld refinement was performed using software Jana2006,[17] as shown in Figure S1.

**In Situ Experiments and Density Functional Theory Calculations.** We used a diamond anvil cell (DAC) equipped with diamonds with a culet size of 400 $\mu$m in diameter to generate high pressure. Type-IIa diamond anvils were used for the IR experiment. T-301 stainless steel gaskets were preindented to about 30 $\mu$m in thickness, and a hole with $d$ = 180 $\mu$m was drilled at the center of the indentation to serve as a sample chamber. All the samples were loaded into the glovebox, and no pressure transmitting medium was used to avoid any possible protonation. A ruby ball was used to calibrate the pressure.[18]

The in situ Raman experiment was performed on a Renishaw micro-Raman spectroscopy system equipped with a second-harmonic Nd:YAG laser ($\lambda$ = 532 nm). The Raman spectra were recorded with a backscattering configuration, and a 2400 lines/mm grating was used. In situ infrared spectra were collected on a Bruker VERTEX 70v system with a HYPERION 2000 microscope. A Globar was used as a conventional source, and the spectra were collected in the transmission mode with a range of 600−4000 $cm^{-1}$ through an aperture of 20 × 20 $\mu m^2$. A resolution of 2 $cm^{-1}$ was applied, and the absorption of the same region of the diamond anvils was used as the background for data reduction.

The in situ powder XRD experiment under high pressure was performed on the 5A XRS-MS beamline at the Pohang Accelerator Laboratory (PAL). The wavelength of the incident X-ray beam was 0.69265 Å. The beam size was collimated to 30 $\mu$m × 30 $\mu$m using a double pinhole collimator. A Mar 345 image plate detector calibrated by $CeO_2$ was used to collect diffraction data, and the exposure time was 180 s for every data point. The Dioptas[19] and Jana 2006[17] programs were used for data reduction and Rietveld refinement, respectively.

Density functional theory (DFT) calculations were conducted to optimize the crystal structure of $NaC_2H$ under high pressure, complementing the Rietveld refinement result. Structural optimization under diverse pressures was implemented with the Vienna Ab initio Simulation Package (VASP) code, using the projector-augmented plane-wave (PAW) method.[20−22] The PAW pseudopotentials were used with the generalized gradient approximation (GGA) and the Perdew−Burke−Ernzerhof (PBE) exchange-correlation function.[23] A cutoff energy of 600 eV was performed with a $k$-point sampling of less than $2\pi \times 0.03$ $A^{-1}$.

Impedance spectroscopy was measured on a Solartron 1260 impedance analyzer and Solartron 1296 dielectric interface. A stainless steel-supported boron nitride (BN) gasket was preindented to a thickness ($L$) of 27 $\mu$m, and a hole with $d$ = 180 $\mu$m was drilled at the center of the indentation to act as the sample chamber. Two Pt foil electrodes were mounted on the two diamonds respectively in a parallel-plate configuration. The applied ac voltage was 100 mV, and the frequency range was from 32 MHz to 80 Hz.

**Ex Situ Gas Chromatography−Mass Spectrometry (GC−MS) Measurements.** The sample used for gas chromatography−mass spectrometry (GC−MS) measurements was synthesized by using a VX3 Paris-Edinburgh (PE) cell equipped with two double-toroidal sintered diamond anvils in the glovebox. $NaC_2H$ (18 mg) was precompressed at about 10 MPa to make a pellet, which was put into an encapsulated stainless steel gasket and moved into the PE cell. An automatic syringe pump was used to drive the PE cell, and the pressure was estimated from the Edinburgh group calibration curve.[24] Then, the sample was compressed to 20 GPa at speeds of 0.04 GPa $min^{-1}$ below 5 GPa, 0.02 GPa $min^{-1}$ from 5 to 10 GPa, 0.01 GPa $min^{-1}$ from 10 to 15 GPa, and 0.005 GPa $min^{-1}$ from 15 to 20 GPa. The sample was maintained at 20 GPa for 1 day and then downloaded to ambient pressure at the same rates. The product (18 mg) was obtained after removing the gaskets.

The high-resolution GC−MS experiment was performed on a Thermo Scientific Q Exactive GC hybrid quadrupole-orbitrap mass spectrometer equipped with an electron ionization (EI) source. The sample synthesized by the PE cell was sealed into a sample vial in the glovebox, and 20 $\mu$L of water was injected into the bottle. The generated gas (0.2 mL) was manually injected into a Thermo Scientific TRACE 1310 GC furnished with a TG-5SilMS capillary column (30 m × 0.25 mm i.d.; 0.25 $\mu$m film thickness). Helium (99.999%) was used as the carrier gas at a constant flow of 1.0 mL $min^{-1}$. The gas was injected in the split mode of 30:1 (v/v) at 150 °C, which is the same temperature of the transfer line. The GC oven was programmed from 30 °C (maintained for 2 min) at a rate of 2 °C $min^{-1}$ to 200 °C (maintained for 2 min). The Q Exactive GC system was operated in the EI mode at 70 eV using a full scan at a resolving power of 30,000 ($m/z$ 200). Scan spectra were recorded in the $m/z$ range of 33−550.

$n$-Hexane (GC grade, ≥ 98%) was added to the hydrolyzation system to extract the nonvolatile molecules for the high-resolution GC−MS experiment. Three parallel experiments were conducted with $n$-hexane as the reference. The sample (1 $\mu$L) was injected manually at 280 °C, which is the same temperature of the ion source and transfer lines. The chromatographic column oven was initially maintained at 40 °C for 2 min and heated to 280 °C at the rate of 5 °C $min^{-1}$ (maintained for 10 min). Scan spectra were recorded in the $m/z$ range of 50−750 using the full scan mode at 60,000 resolving power ($m/z$ 200) mass resolution. The mass spectrometer system was calibrated by the calibration solution to achieve a mass accuracy of <5 ppm root mean square (RMS). Data was lock-mass corrected during the acquisition using a GC column bleed siloxane masses.

All the data were processed using the Thermo Scientific TraceFinder 4.0 software. Thermo Scientific deconvolution software with the National Institute of Standards and Technology (NIST) 2014, Wiley9 Data library, and high-resolution filtering (HRF) were used to process the MS results.[25] The content percentage of each component was calculated by the integral area of the ionic peaks of each compound relative to the total ionic peak.

To carefully determine the fragment intensity of $C_4H_6$ in a small $m/z$ range, a GC−MS experiment on the generated gas



DOI: 10.1021/acs.jpcc.9b09698
J. Phys. Chem. C 2019, 123, 30746−30753

from the hydrolysis of the product synthesized by the PE cell was also performed on an Agilent 7890A/5975C. An HP-5 capillary column (60 m × 0.25 mm i.d.; 0.25 μm film thickness) was used for separation. Before adding water, argon in the sample vial was replaced by helium to reduce the interference because the formula weight of Ar is the same as that of $C_4H_6$. The gas (10 μL) was injected manually in the splitless mode at 150 °C, which is the same temperature as the ion source. The GC oven was programmed from 33 °C (hold time, 10 min) at 3 °C $min^{-1}$ to 50 °C (hold time, 2 min). The MS was operated in the EI mode with the ion source temperature of 150 °C, and the transfer line was set at 200 °C. The mass was calibrated by perfluorotributylamine. Scan spectra were recorded in the *m/z* range of 33−150, and MSD ChemStation data analysis software was used for data acquisition and analysis. Wiley Registry 10th Edition/NIST 2014 EI library was used for the spectral library search.

## RESULTS AND DISCUSSION

In situ Raman spectra of monosodium acetylide up to 16.7 GPa in the range of 1500−2300 $cm^{-1}$ are shown in Figure 1a.

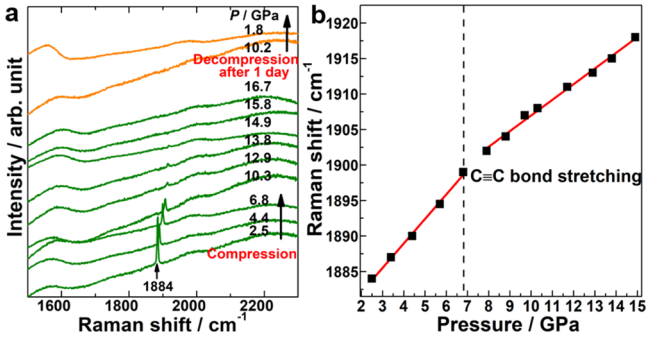


**Figure 1.** (a) Selected Raman spectra of $NaC_2H$ upon compression and decompression. (b) Frequency shifts of the C≡C bond stretching mode as a function of pressure. The vertical line indicates the boundaries of the different phases.

No obvious peaks were observed outside this range (Figure S2). The peak at 1884 $cm^{-1}$ (at 2.5 GPa) is ascribed to the stretching of the C≡C bond, which blue-shifts under compression due to the enhancement of interatomic interactions. The peak shifts at different rates below and above 7 GPa (Figure 1b), which indicates a second-order phase transition. Above 14.9 GPa, this Raman peak degrades and disappears, which suggests the polymerization of triple bonds. After preservation at 16.7 GPa for 1 day, the sample was decompressed, and no Raman peaks were observed during the whole decompression process. This suggests that the reaction of the C≡C bond is irreversible.

Infrared (IR) absorption spectroscopy provides complementary information, which avoids the influence of fluorescence and gives more bonding information. The in situ IR measurements were carried out up to 30.1 GPa, as shown in Figure 2. All the peaks were blue-shifted and broadened under compression (Figure 2a). At 15.4 GPa, a new peak appeared in the high-frequency side of the antisymmetric C−H bending vibration centered at 660 $cm^{-1}$. At 16.9 GPa, the peak centered at 1880 $cm^{-1}$ (C≡C stretching) broadens, and the intensity of the antisymmetric C−H stretching vibration centered at 3238 $cm^{-1}$ obviously decreases, which corresponds to the reaction of the C≡C bond. At about 30 GPa, all the $NaC_2H$ peaks

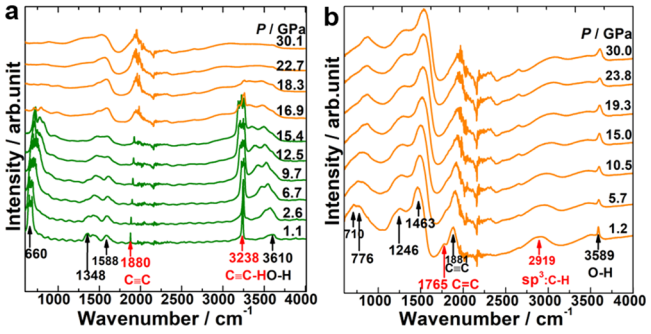


**Figure 2.** Selected infrared absorption spectra of $NaC_2H$ upon (a) compression and (b) decompression. The peak at 3610 $cm^{-1}$ is recognized as the O−H stretching from NaOH impurities.

disappeared, indicating a complete reaction. After maintaining the $NaC_2H$ at 30 GPa for 1 day and decompressing it to 1.2 GPa, several new, broad peaks at 776, 1246, 1463, 1765, and 2919 $cm^{-1}$ were observed (Figure 2b). The peak centered at 2919 $cm^{-1}$ (1.2 GPa) is in the region of C($sp^3$)−H stretching, which demonstrates that $NaC_2H$ polymerized under high pressure and the carbon with sp hybridization transformed to $sp^3$.

To understand the connection of the carbon atoms in the product, we protonated the carbon network formed under high pressure by adding water to the recovered sample and investigated the hydration product by GC−MS. As shown in Figure 3, three parallel experiments were conducted for comparison: air (Figure 3a), gas released from the hydration of the starting material (Figure 3b) for the reference, and gas released from the hydration of the sample recovered from 20 GPa (Figure 3c). The hydrolysis of the recovered sample follows this reaction equation: $C_xH_y^{n-}$ (s) + $nH^+$ = $C_xH_{y+n}$ (g). $C_xH_y^{n-}$ anions in the solid state react with $nH^+$ from $H_2O$ to generate the gas $C_xH_{y+n}$ for GC−MS detection. The molecular formula of most peaks in the total ion chromatograms (TICs) was determined unambiguously, as listed in Table 1. The gas from the raw material almost only contains $C_4H_2$, which is the product of acetylene dimerization in the mass spectrometer (after GC). For the sample recovered from 20 GPa, the hydration product includes $C_3H_4$, $C_4H_6$, $C_4H_2$, $C_5H_6$, $C_6H_6$, $C_6H_8$, $C_7H_6$, $C_8H_6$, $C_8H_8$, and $C_8H_{10}$ in the gas phase, with various isomers. These molecules were absent in the gas released from the raw material and thus demonstrated the polymerization. The C/H ratio of the advanced hydrocarbons is still around 1:1, with $x - 2 \le y + n \le x + 2$, which suggests that the PIP process is accompanied by some certain disproportionation reactions but not a significant phase separation similar to that in the PIP of $Li_2C_2$.[13] This indicates that in the PIP of $NaC_2H$, $Na^+$ does not remotely diffuse and the sample does not form Na-rich and C-rich phases similar to the formation of $Li_4C_3$, $Li_6C_3$, and $Li_3C_4$ in the PIP of $Li_2C_2$.[13]

These gas molecules are most likely to be unsaturated and were analyzed by searching the NIST library. The possible candidates with a fitting score over 500 are presented in Table 1. The candidates include both linear and cyclic molecules, which suggest that the carbon framework in the polymerized $NaC_2H$ also includes such fragments. Three main components in the gas product are $C_3H_4$, $C_4H_6$, and $C_4H_2$, occupying over 87% of the total products (Figure 3d). $C_3H_4$ was also identified in the hydration product of the PIP of $CaC_2$[15] and was arguably recognized as cyclopropene here (Figure 3e and


DOI: 10.1021/acs.jpcc.9b09698
J. Phys. Chem. C 2019, 123, 30746−30753

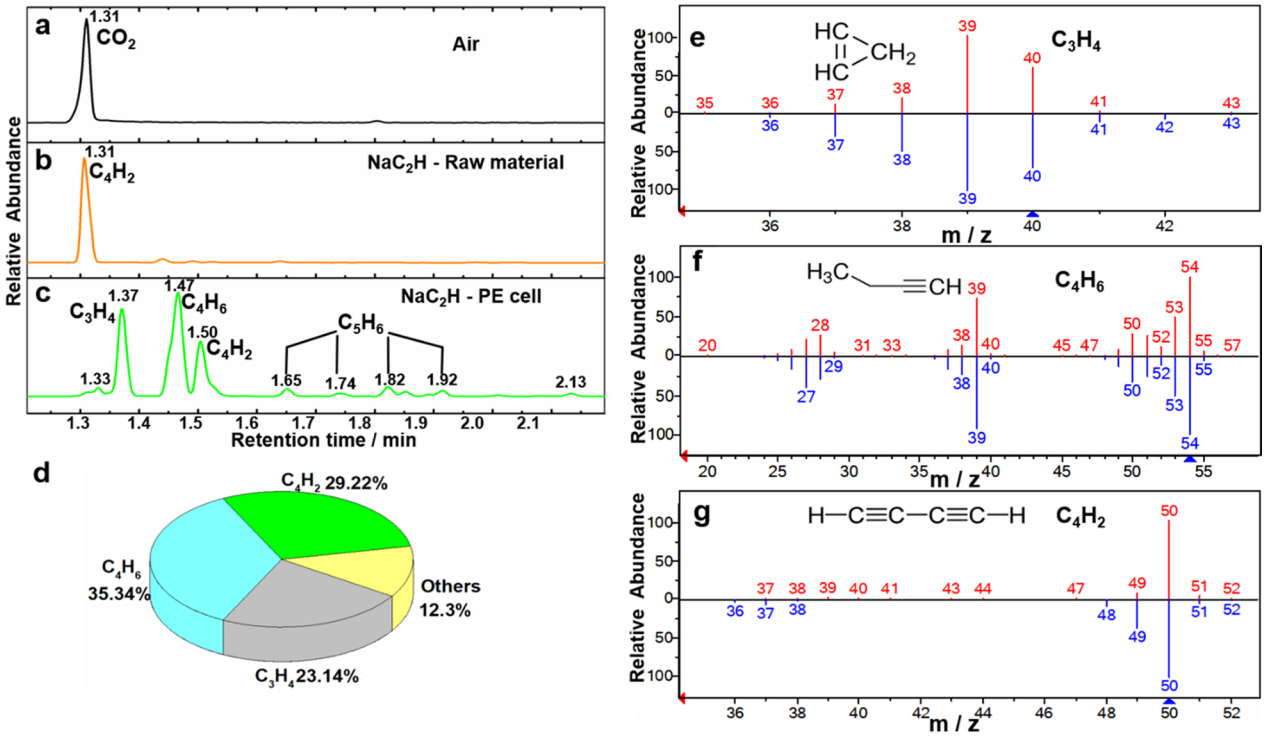


**Figure 3.** Selected total ion chromatograms (TICs) of (a) air, (b) hydrolysis product of $NaC_2H$ raw material, and (c) hydrolysis product of the recovered $NaC_2H$ from 20 GPa. (d) Percentage of the components in the hydrolysis products. The cyan, green, gray, and yellow slices represent $C_4H_6$, $C_4H_2$, $C_3H_4$, and others, respectively. The mass spectra comparison with NIST spectra: (e) $C_3H_4$ and cyclopropene, (f) $C_4H_6$ (collected on Agilent 7890A-5975C) and 1-butyne, and (g) $C_4H_2$ and 1,3-butadiyne. The red bars are the experimental results, and the blue bars are the NIST standard spectra.

**Table 1. Selected High-Resolution Mass Spectrum Results Obtained by Deconvolution**

| retention time (min) | formula | *m/z* (Da) | Δppm | percent (%) | name (NIST and Wiley) | fitting score |
|---|---|---|---|---|---|---|
| 1.37 | $C_3H_4$ | 40.0313 | 3.040 | 23.14 | cyclopropene | 822 |
| 1.47 | $C_4H_6$ | 54.0469 | 0.892 | 35.34 | 1-butyne | 926[a] |
| | | | | | 1,3-butadiene | 889[a] |
| 1.50 | $C_4H_2$ | 50.0156 | 0.633 | 29.22 | 1,3-butadiyne | 704 |
| 1.66 | $C_5H_6$ | 66.0469 | 0.579 | 0.78 | 2-methyl-1-buten-3-yne | 585 |
| 1.74 | $C_5H_6$ | 66.0469 | 1.033 | 0.52 | 3-penten-1-yne | 508 |
| 1.82 | $C_5H_6$ | 66.0469 | 0.276 | 1.08 | cyclopropylacetylene | 641 |
| 1.92 | $C_5H_6$ | 66.0469 | 0.633 | 1.15 | | |
| 2.52 | $C_6H_8$ | 80.0626 | 4.123 | 1.46 | 1,3-cyclohexadiene | 591 |
| 3.20 | $C_6H_6$ | 78.0469 | 1.176 | 0.63 | 1,5-hexadiyne | 529 |
| 3.50 | $C_6H_8$ | 80.0626 | 0.647 | 0.63 | 3-methylenecyclopentene | 598 |
| 3.71 | $C_6H_8$ | 80.0626 | 1.397 | 0.98 | 5-methyl-1,3-cyclopentadiene | 512 |
| 4.47 | $C_7H_6$ | 90.0469 | 0.536 | 1.71 | bicyclo[4.1.0]hepta-1,3,5-triene | 505 |
| 6.40 | $C_8H_{10}$ | 106.0783 | 4.437 | 0.85 | | |
| 9.15 | $C_8H_8$ | 104.0626 | 1.370 | 0.60 | 1,3,7-octatrien-5-yne | 529 |
| 11.23 | $C_8H_8$ | 104.0626 | 0.367 | 1.00 | 1,3,5,7-cyclooctatetraene | 545 |
| 13.22 | $C_8H_6$ | 102.0469 | 1.550 | 0.91 | | |

[a]The data for substance identification was collected on the Agilent GC−MS.

Figure S3). The reason for forming such an unstable molecule is still under investigation, but it must result from the dissociation of some complex carbon structure during the decompression or hydrolysis process. $C_4H_6$ has many isomers and is finally recognized as 1-butyne (Figure 3f and Figure S4) by carefully determining the fragment abundance in the small *m/z* range, but 1,3-butadiene cannot be excluded solely by the MS. $C_4H_2$ is recognized as 1,3-butadiyne (Figure 3g). Its retention time is different from that observed in the hydrolysis product of $NaC_2H$ because it is in the gas sample before it is injected into GC. It results from the hydration of $^-C{\equiv}C{-}C{\equiv}C^-$, which is generated by the dimerization of two $H{-}C{\equiv}C^-$ anions and a following loss of hydrogen atoms. The coexistence of $C_4H_6$ and $C_4H_2$ and lack of $C_4H_4$ indicate a disproportionation reaction, with the composition of the product still in the range of $C_xH_{x\pm2}$. This disproportionation is most likely due to the pairing of the free radicals by adding or losing two hydrogen atoms, such as $2{\cdot}C(H){=}C(H){-}C(H){=}C(H){\cdot} \rightarrow C_4H_6 + C_4H_2$, where (H) means a possible connection to H.



DOI: 10.1021/acs.jpcc.9b09698
J. Phys. Chem. C 2019, 123, 30746−30753

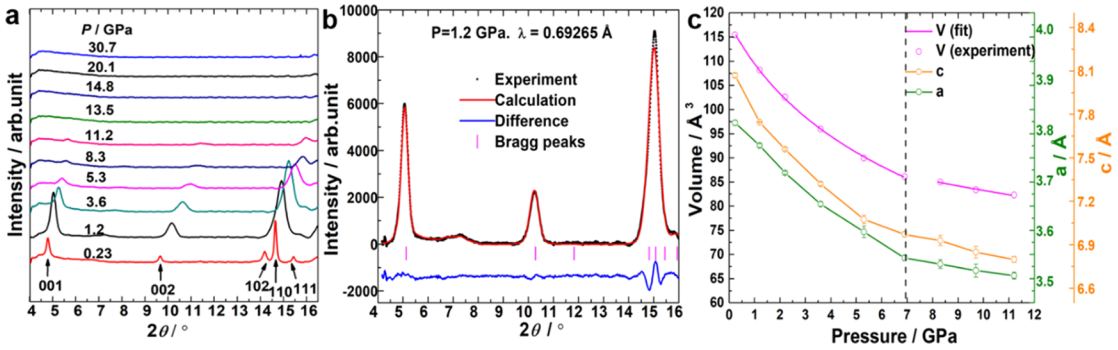


**Figure 4.** (a) Selected in situ XRD patterns of $NaC_2H$ under compression. (b) Rietveld refinement plot of the $NaC_2H$ samples at 1.2 GPa. (c) Evolution of lattice parameters and unit cell volume of $NaC_2H$ under high pressure. The solid line represents the fitting results of the third-order Birch−Murnaghan equation of state.

The hydrolysis product extracted by hexane is shown in Figure S5, and many isomers of $C_8H_{10}$ and $C_{10}H_{10}$ were identified (Table S1). The total content of $C_8H_{10}$ is nearly 60% and that of $C_{10}H_{10}$ is nearly 32% (Figure S5d). The C/H ratio of most hydrocarbons is also around 1:1, meaning that the degree of unsaturation of the PIP products did not change, and the charges are evenly distributed in the carbon skeleton. *p*-Xylene, *o*-xylene, 3-butynylbenzene, and several other aromatic compounds are suggested (Table S1), which indicates that the PIP of NaCCH tend to form cyclic products. For comparison, the PIP product of $CaC_2$ above 20 GPa release $C_3H_4$, $C_5H_6$, $C_5H_4$, $C_6H_4$, $C_6H_6$, $C_6H_8$, $C_{12}H_{10}$, $C_{12}H_{12}$, and $C_{12}H_{14}$ during hydrolysis.[15] Their composition $C_xH_{y+n}$ ($y = 0$) are also in the range of $x - 2 \le y + n \le x + 2$, which suggests that the reaction mechanisms are similar, as discussed later.

To understand the reaction process from a topochemical view, the structural evolution of $NaC_2H$ was investigated by in situ XRD up to 30 GPa (Figure 4a). The crystal structure of $NaC_2H$ is tetragonal with the *P*4/*nmm* space group at ambient conditions.[26] During compression, all the peaks shift to a high angle, broaden, and disappear at 13.5 GPa, and no new peak was observed up to 30 GPa. This corresponds to the polymerization of $NaC_2H$, in agreement with the spectroscopic results shown above.

The lattice parameters below 11 GPa were determined by Rietveld refinement using the $NaC_2H$-*P*4/*nmm* structural model (Figure 4b for 1.2 GPa and Figure S6 for 6.9 GPa). The refined lattices are shown in Figure 4c, and the relationship between the pressure and volume was fitted by the third-order Birch−Murnaghan (B−M) equation of state (EOS)

$$P(V) = \frac{3}{2}B_0\left[\left(\frac{V_0}{V}\right)^{7/3} - \left(\frac{V_0}{V}\right)^{5/3}\right]\left\{1 + \frac{3}{4}(B_1 - 4)\left[\left(\frac{V_0}{V}\right)^{2/3} - 1\right]\right\}$$

$V_0$ is the unit cell volume at 0 GPa, and $B_0$ and $B_1$ are the ambient bulk modulus and its derivatives, respectively. The attempt to fit the data below and above 6.9 GPa by one curve does not result in reasonable values, and two curves were chosen to fit the data (Figure 4c). In the range of 0.2−6.9 GPa, the fitting results are $V_0 = 118.0 \pm 0.8$ Å$^3$, $B_0 = 11.5 \pm 1.0$ GPa, and $B_1 = 4.0 \pm 0.4$. In the range of 7−11.2 GPa, $B_1$ is fixed to 4, and the fitting results are $V_0 = 95.9 \pm 1.9$ Å$^3$ and $B_0 = 53.2 \pm 9.7$ GPa. The $V_0$ above 7 GPa becomes much smaller, while $B_0$ becomes much larger, which means that $NaC_2H$ becomes much denser and less compressive after the phase transition.

The atomic positions are optimized theoretically with the lattice parameters fixed at the experimental value. The intermolecular carbon−carbon distances are compressed under external pressure. $d_1$, $d_2$, and $d_3$ represent the three nearest carbon−carbon distances, as shown in Figure 5a. All of them decrease with increasing pressure, and $d_3$ decreases faster than the others, which is around 3.0 Å at 11 GPa (Figure 5b) or at around 2.9 Å if we extrapolate the curve to the polymerization pressure at 14 GPa. This indicates that the reaction most likely takes place along the $d_3$ direction. The distance is similar to that of $CaC_2$. $CaC_2$ has a monoclinic structure ($CaC_2$-VI) above 10 GPa.[15] As optimized by theoretical investigations, the nearest intermolecular carbon−carbon distance is around 2.84 Å at a reaction threshold of 19 GPa, as shown in Figure S7. Considering the temperature effect, the threshold for the reaction between the acetylide anions should be around 2.9 Å. For the PIP pressure, $C_2^{2-}$ in $CaC_2$ has two negative charges, while $C_2H^-$ in $NaC_2H$ has only one, so it will need more force to make $C_2^{2-}$ move closer to each other and result in a much higher PIP pressure. Also, for comparison, $C_2H_2$ has no charge, and an external pressure of 3.5 GPa is enough to drive the polymerization.[16] Hence, we can conclude that the higher the charge density, the higher the polymerization pressure, based on the experimental data.

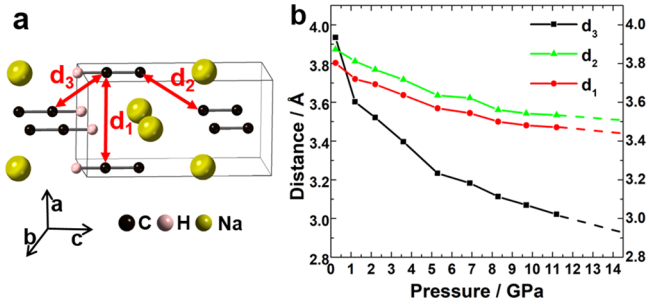


**Figure 5.** (a) Crystal structure of $NaC_2H$. $d_1$, $d_2$, and $d_3$ represent different intermolecular C···C distance. (b) Evolution of $d_1$, $d_2$, and $d_3$ as a function of pressure.

For the proposed PIP reaction starting between the two adjacent CH groups, their bonding along $d_3$ is also energetically favored due to the less electrostatic repulsion than the other end of the $^-C{\equiv}CH$ anion (Figure 5a). For such a



DOI: 10.1021/acs.jpcc.9b09698
J. Phys. Chem. C 2019, 123, 30746−30753

**Scheme 1. Proposed Reaction Routes of the Dimerization and the Following H-Transfer Process**

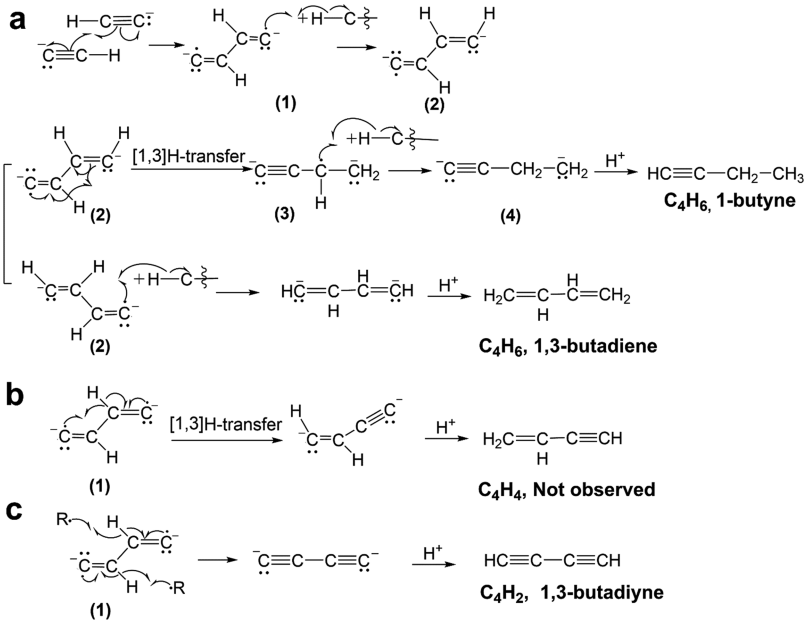


dimerization, a diradical anion $\cdot:^{-}C{=}CH{-}CH{=}C^{-}:\cdot$ (1) will be generated, with the two negative charges and two radicals at the ends of the chain. This anion is not stable and will transform to closed-shell anions by absorbing or losing hydrogen atoms and then transfer to $C_4H_2$ and $C_4H_6$ after protonation, which is consistent with the GC−MS results.

The reaction routes are proposed in Scheme 1, with the assumption that the negative charges stay at the ends of the chain, and the negatively charged carbon atoms are protonated without other reactions (rearrangement). The diradical anion $C_4H_2^{2-}$ (1) will absorb a hydrogen atom and have a radical paired, forming $\cdot C_4H_3^{2-}$ (2). If (2) experiences a [1,3] H-transfer and produces (3) with the radical transferred to the secondary carbon, the absorption of the second hydrogen will result in (4) with an ethynide end and an alkylide end, which will result in 1-butyne (first reaction route in a). If (2) absorb the second hydrogen directly, $^{-}CH{=}CH{-}CH{=}CH^{-}$ will be formed, which will result in 1,3-butadiene by protonation (second reaction route in a). It should be noted that (4) is consistent with the IR result, which shows a clear $C(sp^3)$−H vibration signal, and is most likely the real process. If (1) experienced a [1,3] H-transfer following the route b, the product would form $H_2C{=}CH{-}C{\equiv}CH$ after protonation, which was not observed in the MS result and suggested that this intramolecular pairing route of diradicals is not favored. On the other hand, losing a H atom will also stabilize (1) by pairing the radicals and forming a triple bond, and losing the second H atom will result in the 1,3-butadiyne dianion $C_4^{2-}$ (route c). From the above analysis, we can understand why the hydrolysis products always have a C/H ratio within $C_xH_{x\pm2}$. This is because the produced species need to absorb or lose at most two hydrogen atoms for pairing their two radicals.

The in situ impedance spectroscopy of $NaC_2H$ was also measured up to 31 GPa (Figure 6). The resistance below 10 GPa was beyond the instrument limit under compression. From 10 to 31 GPa, the thickness of the sample chamber changed from 27 to 12 $\mu$m, and the diameter changed from 245 to 170 $\mu$m. Assuming that the thickness and diameter vary linearly with pressure under compression, the resistivity is

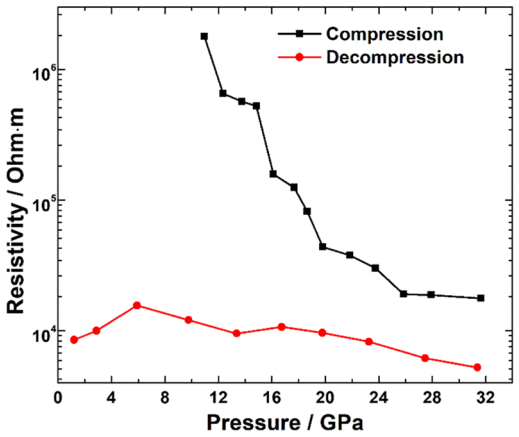


**Figure 6.** Electrical resistivity of $NaC_2H$ during compression and decompression.

calculated and decreased more than 100 times from 10 to 31 GPa. After 1 day, the resistivity decreased from $1.8 \times 10^4$ to $5.2 \times 10^3$ Ω·m as the polymerization occurred more completely. During the decompression process, the resistivity is around $10^4$ Ω·m. This irreversibility is most likely due to the formation of covalent bonds between the acetylide anions.

## CONCLUSIONS

In summary, we used in situ Raman, IR, XRD, impedance spectroscopy, and ex situ GC−MS to determine the phase transition and polymerization of $NaC_2H$ under high pressure. $C_2H^-$ polymerizes at about 14 GPa, which is much lower than those of other metal acetylides and already in the working range of typical large volume press. This reaction pressure is between those of $C_2H_2$ (3.5 GPa) and $CaC_2$ (22 GPa), which shows that the charge of the monomer is positively related to the polymerization pressure. The reaction threshold of the intermolecular carbon−carbon distance is determined as about 2.9 Å, which is similar to that of $CaC_2$ and, hence, suggests its popularity. The topochemical initiation mechanism and subsequent H-transfer process are proposed based on the



DOI: 10.1021/acs.jpcc.9b09698
J. Phys. Chem. C 2019, 123, 30746−30753

crystal structure and the GC−MS results. Additionally, similar to the PIP of $CaC_2$, the conductivity of $NaC_2H$ was significantly and irreversibly enhanced under external pressure. This demonstrated that the PIP of the C≡C triple bond species, including those carrying charges and substituted groups, is a promising method to synthesize novel polymeric metal−organic conductors. Our investigations provide helpful insight to understand these processes.

## ■ ASSOCIATED CONTENT

### Supporting Information

The Supporting Information is available free of charge at https://pubs.acs.org/doi/10.1021/acs.jpcc.9b09698.

Rietveld refinement plot of the $NaC_2H$ at ambient pressure (Figure S1); selected Raman spectra of $NaC_2H$ in the range of 50−1300 $cm^{-1}$, 2050−3100 $cm^{-1}$ and 3080−3900 $cm^{-1}$ upon compression (Figure S2); comparison between the mass spectrometry data of $C_3H_4$ and that in NIST 2014, Wiley9 Data library (Figure S3); selected total ion chromatograms (TICs) of the hydrolysis $NaC_2H$ recovered from 20 GPa (Figure S4) and the hydrolyzed sample extracted by hexane (Figure S5); Rietveld refinement plot of the $NaC_2H$ at 6.9 GPa (Figure S6); carbon−carbon distance of the $CaC_2$-I at 19 GPa and 298 K and the new phase $CaC_2$-VI predicted by theoretical calculation at 19 GPa and 0 K (Figure S7); selected high-resolution mass spectrum results obtained by deconvolution of the hydrolyzed sample extracted by hexane (Table S1) (PDF)

## ■ AUTHOR INFORMATION


### Corresponding Authors

*E-mail: zhenghy@hpstar.ac.cn (H.Z.).
*E-mail: likuo@hpstar.ac.cn (K.L.).

### ORCID

Yehua Han: 0000-0002-8416-9860
Haiyan Zheng: 0000-0002-4727-5912
Kuo Li: 0000-0002-4859-6099


### Author Contributions

The manuscript was written with contributions from all authors. All authors have approved the final version of the manuscript.

### Notes

The authors declare no competing financial interest.

## ■ ACKNOWLEDGMENTS

This research is supported by the National Natural Science Foundation of China (NSFC) (grant nos. 21771011 and 21875006). The authors also acknowledge the support from the Top 1000-Talents Award.

## ■ REFERENCES


(1) Weller, T. E.; Ellerby, M.; Saxena, S. S.; Smith, R. P.; Skipper, N. T. Superconductivity in the Intercalated Graphite Compounds $C_6Yb$ and $C_6Ca$. *Nat. Phys.* **2005**, *1*, 39−41.

(2) Hebard, A. F.; Rosseinsky, M. J.; Haddon, R. C.; Murphy, D. W.; Glarum, S. H.; Palstra, T. T. M.; Ramirez, A. P.; Kortan, A. R. Superconductivity at 18 K in Potassium-Doped $C_{60}$. *Nature* **1991**, *350*, 600−601.

(3) Kelly, T. G.; Chen, J. G. Metal Overlayer on Metal Carbide Substrate: Unique Bimetallic Properties for Catalysis and Electrocatalysis. *Chem. Soc. Rev.* **2012**, *41*, 8021−8034.

(4) Kurakevych, O. O.; Strobel, T. A.; Kim, D. Y.; Cody, G. D. Synthesis of $Mg_2C$: a Magnesium Methanide. *Angew. Chem., Int. Ed.* **2013**, *52*, 8930−8933.

(5) Srepusharawoot, P.; Blomqvist, A.; Araújo, C. M.; Scheicher, R. H.; Ahuja, R. One-dimensional Polymeric Carbon Structure based on Five-membered Rings in Alkaline Earth Metal Dicarbides $BeC_2$ and $MgC_2$. *Phys. Rev. B* **2010**, *82*, 125439.

(6) Chen, X.-Q.; Fu, C. L.; Franchini, C. Polymeric Forms of Carbon in Dense Lithium Carbide. *J. Phys.: Condens. Matter* **2010**, *22*, 292201.

(7) Benson, D.; Li, Y.; Luo, W.; Ahuja, R.; Svensson, G.; Häussermann, U. Lithium and Calcium Carbides with Polymeric Carbon Structures. *Inorg. Chem.* **2013**, *52*, 6402−6406.

(8) Li, Y. L.; Wang, S. N.; Oganov, A. R.; Gou, H.; Smith, J. S.; Strobel, T. A. Investigation of Exotic Stable Calcium Carbides using Theory and Experiment. *Nat. Commun.* **2015**, *6*, 6974.

(9) Li, Y.-L.; Luo, W.; Zeng, Z.; Lin, H.-Q.; Mao, H.-k.; Ahuja, R. Pressure-induced Superconductivity in $CaC_2$. *Proc. Natl. Acad. Sci. U. S. A.* **2013**, *110*, 9289−9294.

(10) Zhang, C.; Lan, J.; Jiang, H.; Li, Y.-L. Stable and Metastable Structures in Compressed $LiC_6$: Dimensional Diversity. *J. Phys. Chem. C* **2016**, *120*, 10137−10145.

(11) Lin, Y.; Strobel, T. A.; Cohen, R. E. Structural Diversity in Lithium Carbides. *Phys. Rev. B* **2015**, *92*, 214106.

(12) Profeta, G.; Calandra, M.; Mauri, F. Phonon-mediated Superconductivity in Graphene by Lithium Deposition. *Nat. Phys.* **2012**, *8*, 131−134.

(13) Wang, L.; Dong, X.; Wang, Y.; Zheng, H.; Li, K.; Peng, X.; Mao, H.-k.; Jin, C.; Meng, Y.; Huang, M.; et al. Pressure-induced Polymerization and Disproportionation of $Li_2C_2$ Accompanied with Irreversible Conductivity Enhancement. *J. Phys. Chem. Lett.* **2017**, *8*, 4241−4245.

(14) Dong, X.; Wang, L.; Li, K.; Zheng, H.; Wang, Y.; Meng, Y.; Shu, H.; Mao, H. -k.; Feng, S.; Jin, C. Tailored Synthesis of the Narrowest Zigzag Graphene Nanoribbon Structure by Compressing the Lithium Acetylide under High Temperature. *J. Phys. Chem. C* **2018**, *122*, 20506−20512.

(15) Zheng, H.; Wang, L.; Li, K.; Yang, Y.; Wang, Y.; Wu, J.; Dong, X.; Wang, C.-H.; Tulk, C. A.; Molaison, J. J.; et al. Pressure Induced Polymerization of Acetylide Anions in $CaC_2$ and $10^7$ Fold Enhancement of Electrical Conductivity. *Chem. Sci.* **2017**, *8*, 298−304.

(16) Aoki, K.; Usuba, S.; Yoshida, M.; Kakudate, Y.; Tanaka, K.; Fujiwara, S. Raman Study of the Solid-State Polymerization of Acetylene at High Pressure. *J. Chem. Phys.* **1988**, *89*, 529−534.

(17) Petříček, V.; Dušek, M.; Palatinus, L. Crystallographic Computing System JANA2006: General Features. *Z. Kristallogr.-Cryst. Mater.* **2014**, *229*, 345−352.

(18) Mao, H. K.; Xu, J.; Bell, P. M. Calibration of the Ruby Pressure Gauge to 800 kbar under Quasi-hydrostatic Conditions. *J. Geophys. Res.: Solid Earth* **1986**, *91*, 4673−4676.

(19) Prescher, C.; Prakapenka, V. B. DIOPTAS: a Program for Reduction of Two-dimensional X-ray Diffraction Data and Data Exploration. *High Pressure Res.* **2015**, *35*, 223−230.

(20) Kresse, G.; Hafner, J. Ab Initio Molecular Dynamics for Liquid Metals. *Phys. Rev. B* **1993**, *47*, 558−561.

(21) Kresse, G.; Furthmüller, J. Efficiency of Ab-initio Total Energy Calculations for Metals and Semiconductors Using a Plane-wave Basis Set. *Comput. Mater. Sci.* **1996**, *6*, 15−50.

(22) Kresse, G.; Joubert, D. From Ultrasoft Pseudopotentials to the Projector Augmented-wave Method. *Phys. Rev. B* **1999**, *59*, 1758−1775.

(23) Perdew, J. P.; Burke, K.; Ernzerhof, M. Generalized Gradient Approximation Made Simple. *Phys. Rev. Lett.* **1996**, *77*, 3865−3868.

(24) Salmon, P. S.; Drewitt, J. W. E.; Whittaker, D. A. J.; Zeidler, A.; Wezka, K.; Bull, C. L.; Tucker, M. G.; Wilding, M. C.; Guthrie, M.; Marrocchelli, D. Density-driven Structural Transformations in Network Forming Glasses: a High-pressure Neutron Diffraction




DOI: 10.1021/acs.jpcc.9b09698
J. Phys. Chem. C 2019, 123, 30746−30753

Study of $GeO_2$ Glass up to 17.5 GPa. *J. Phys.: Condens. Matter* **2012**, *24*, 439601.
(25) Kwiecien, N. W.; Bailey, D. J.; Rush, M. J. P.; Cole, J. S.; Ulbrich, A.; Hebert, A. S.; Westphall, M. S.; Coon, J. J. High-resolution Filtering for Improved Small Molecule Identification via GC/MS. *Anal. Chem.* **2015**, *87*, 8328−8335.
(26) Atoji, M. Neutron Structure Determination of Monosodium Acetylide, $NaC_2H$, at 293 and 5° K. *J. Chem. Phys.* **1972**, *56*, 4947−4951.



DOI: 10.1021/acs.jpcc.9b09698
*J. Phys. Chem. C* 2019, 123, 30746−30753